Table 1. *Comparison of estimated positive and negative triplets according to our formula and to the Kronenburg formula*

nr and nw are the numbers of estimated triplets and of wrongly estimated triplets, respectively; f.s.p. is the fraction of scattering power corresponding to the atoms involved in the triangles.

	Our formula [(6)]				Kronenburg formula			
	Positive triplets		Negative triplets		Positive triplets		Negative triplets	
	nr	nw	nr	nw	nr	nw	nr	nw
(*a*) CUPP ($Cu_2Br_2P_4C_{88}H_{68}$)								
56 Cu-atom triangles f.s.p. = 0.21	7904	20	96	90	7256	18	744	736
56 Br-atom triangles f.s.p. = 0.30	7976	2	24	0	7898	2	102	78
(*b*) AGI ($Ag_2I_2P_4C_{64}H_{56}$)								
56 Ag-atom triangles f.s.p. = 0.33	7915	12	85	82	7489	6	511	502
56 I-atom triangles f.s.p. = 0.42	7945	8	55	48	7688	4	312	301
560 Ag + I-atom triangles f.s.p. = 0.75	7988	3	12	0	7965	0	35	20

to overestimate triplet negativity is also supported. These conclusions are confirmed by the following additional test.

For AGI, 8000 triplet invariants among the 486 largest $|E|$ were selected by *SIR*92: 15 triplets are really negative. The value of G was calculated by including in $\beta_{\mathbf{u}_1,\mathbf{u}_2}$ all the 56 interatomic triangles corresponding to Ag atoms (f.s.p. = 0.33); calculations were then repeated by including iodine triangles (f.s.p. = 0.42). At the end, we calculated G by including in $\beta_{\mathbf{u}_1,\mathbf{u}_2}$ all the 560 interatomic triangles corresponding to I and Ag atoms (f.s.p. = 0.75).

Concluding remarks

A probabilistic approach has been described that is able to take into account prior information on interatomic triangles that may be available after inspection of a Patterson map. The procedure generalizes the so-called vector-interaction formula of Hauptman & Karle (1962) and provides a final formula different from a previous probabilistic expression derived by Kronenburg (1992). The three methods are compared: our probabilistic approach overcomes some theoretical limitations of the algebraic method and improves triplet estimates provided by the Kronenburg formula. Practical tests show also that our triplet estimates are markedly better than Cochran–Woolfson estimates, provided the electron density involved in the interatomic triangles is a non-negligible percentage of the total electron density.

Thanks are due to Miss C. Chiarella for technical support.

References

ALTOMARE, A., CASCARANO, G. & GIACOVAZZO, C. (1992*a*). *Acta Cryst.* A**48**, 30–36.
ALTOMARE, A., CASCARANO, G. & GIACOVAZZO, C. (1992*b*). *Acta Cryst.* A**48**, 495–500.
ALTOMARE, A., CASCARANO, G., GIACOVAZZO, C., GUAGLIARDI, A., BURLA, M. C., POLIDORI, G. & CAMALLI, M. (1994). *J. Appl. Cryst.* **27**, 435.
CAMALLI, M., CARUSO, F. & VENANZI, L. M. (1985). Unpublished work.
CAMALLI, M., CARUSO, F. & VENANZI, L. M. (1986). Unpublished work.
GIACOVAZZO, C. (1991). *Acta Cryst.* A**47**, 256–263.
HAUPTMAN, H. & KARLE, J. (1962). *Acta Cryst.* **15**, 547–550.
KRONENBURG, M. J. (1992). Thesis. Univ. of Amsterdam, The Netherlands.
KRONENBURG, M. J., PESCHAR, R. & SCHENK, H. (1991). *Acta Cryst.* A**47**, 469–480.
KROON, J. & KRABBENDAM, H. (1970). *Acta Cryst.* B**26**, 312–314.
SAYRE, D. (1953). *Acta Cryst.* **6**, 430–431.

Acta Cryst. (1994). A**50**, 588–595

Asymmetric Tilt Boundaries in Polycrystalline Nickel

BY VALERIE RANDLE

Department of Materials Engineering, University College, Swansea SA2 8PP, Wales

(*Received* 30 *July* 1993; *accepted* 14 *March* 1994)

Abstract

A large sample population of grain-boundary geometries in annealed polycrystalline nickel has been collected and analysed. The data include all five degrees of freedom, that is, the grain misorientation plus the crystallographic orientation of the boundary plane. The most significant category of boundaries on the basis of those geometries that could give rise to 'special' properties were symmetric and

asymmetric tilt boundaries in the $\Sigma = 3$ system. Together, these accounted for nearly half the sampled boundaries. Certain plane combinations occurred with an above-average frequency, whereas others, *e.g.* the (211) symmetric tilt boundary, were not observed at all. The data were compatible with recent calculations on the energies of asymmetric tilt boundaries. Furthermore, there was some correlation between $\Sigma = 3$ boundaries and the inclination of the boundary relative to the specimen surface, which could be explained by grain-boundary area and connectivity arguments.

1. Introduction

The geometrical characterization of grain boundaries and more particularly the relationship between grain boundary and properties has been a strong research area for the past two decades. More recently, the focus of attention has extended to include a larger proportion of experiments conducted on polycrystals rather than bicrystals (Randle, 1993*b*). This is primarily a consequence of new experimental techniques, such as electron back-scatter diffraction (EBSD) in a scanning electron microscope (SEM), and improved data handling (Randle, 1992). There are two important differences between the geometrical characterization of grain boundaries in bicrystals and polycrystals:

(1) The connectivity of boundaries is not relevant for bicrystal samples, whereas it has important consequences for polycrystals.

(2) The orientation of the boundary plane is usually predetermined for bicrystals. For polycrystals, it is unknown and its measurement is more technically challenging than that of the misorientation between interfacing grains.

Special (*i.e.* markedly different from average) grain-boundary properties are associated with low free volume (*e.g.* Fullman, 1951). A first-order indication of a high-angle boundary's propensity for 'special' properties is usually inferred from the misorientation expressed as the coincidence-site-lattice (CSL) index, Σ, where Σ is the reciprocal density of coincidence sites. Since they are periodic, low-Σ boundaries have more chance of exhibiting a 'good fit' (*i.e.* minimal specific free volume) than general boundaries. The misorientation supplies three of the five degrees of freedom belonging to a grain boundary; to specify fully the macroscopic boundary geometry with respect to both interfacing lattices, it is necessary to know also the boundary-plane orientation, which supplies the final two degrees of freedom. For many experimental investigations of grain-boundary geometry in polycrystals, it is common to measure only the misorientation and omit the boundary-plane orientation. This is an oversimplification since the free volume and hence the properties of a boundary are governed by all five degrees of freedom rather than only the three associated with the misorientation (Paidar, 1987).

The properties of a boundary can change dramatically if the boundary-plane inclination is varied while the misorientation remains constant. The most extreme and well known examples of boundary-property variation with inclination for fixed misorientation is that of planes in the $\Sigma = 3$ boundary (twin) where the energy of the 'incoherent twin', which has (112) parallel on the two sides of the boundary, may be two orders of magnitude greater than that of the 'coherent twin', which is interfaced by (111) planes.

The relationship between macroscopic boundary geometry and properties is sometimes complex and is as yet incompletely understood. Some factors are considered to be indicators of 'special' boundary properties: these include low-index boundary planes and/or a small boundary period (Wolf, 1985; Wolf, Ernst, Muschik, Finnis & Fischmeister, 1992). Symmetrical tilt boundaries (STBs) and some asymmetric tilt boundaries (ATBs) and twist boundaries (TBs) fulfil these criteria, as do certain boundaries interfaced by low-index planes that are incommensurate. Various theoretical and high-resolution experimental studies provide information that is more detailed on an atomic level and give insight into the hierarchy of 'special' boundary properties and geometries. Taking the relationship between grain-boundary free energy and geometry as an example, it is now known that some ATBs have lower energies than some STBs. This is illustrated in the case of the $\Sigma = 3$ 'family', where there are several ATBs that have lower energy than the (211) STB (Wolf *et al.*, 1992). The (111) STB has the lowest energy of all.

It is clear from the foregoing that STBs, ATBs, TBs and low-index plane (*P*) boundaries form a subgroup of potentially special boundaries that can be identified from a sample population if both the plane indices and the misorientation are known. To date, there have been very few investigations to measure the distribution of grain-boundary plane geometries in polycrystals, whereas there have been many more investigations that show the distribution of grain orientations and misorientations (Furley & Randle, 1991; Crawford & Was, 1991). The present work shows results of grain-boundary plane-geometry analyses in polycrystalline annealed nickel.

2. Experimental

A recrystallized nickel specimen was annealed under vacuum for 2 h at 1273 K to give an average grain size of approximately 170 μm. The specimen was polished and electrolytically etched in 5% sulfuric

Table 1. *Distributions of measured grain-boundary geometries*

Planes	Deviation	Σ	V	Type	Planes	Deviation	Σ	V	Type
(*a*) $\Sigma = 3$ CSLs									
(111)/(111)	1.0°/1.5°		0.23	ST	(411)/(11,5,4)	0.9°/2.4°		0.20	AT
	1.1°/2.6°		0.25	ST	(211)/(744)	1.7°/1.5°		0.15	AT
	1.5°/1.6°		0.28	ST	(210)/(542)	3.7°/2.9°		0.12	AT
	2.2°/3.5°		0.15	ST	(755)/(29,7,1)	2.3°/2.1°		0.03	AT
	2.4°/5.2°		0.62	ST	(711)/(17,11,7)	4.8°/1.5°		0.24	AT
	2.4°/5.2°		0.62	ST	(511)/(13,7,5)	2.6°/2.7°		0.05	AT
(211)/(522)	3.5°/3.7°		0.03	AT	(510)/(431)	2.9°/2.5°		0.03	AT
	1.0°/4.0°		0.36	AT	(510)/(431)	6.5°/6.9°		0.03	AT
	2.4°/4.6°		0.24	AT	(510)/(431)	1.2°/2.7°		0.14	AT
(755)/(23,17,17)	4.1°/2.8°		0.23	AT	(431)/(13,7,4)	1.6°/5.1°		0.34	AT
(332)/(10,7,7)	3.2°/2.2°		0.11	AT	(421)/(11,8,2)	0.6°/0.4°		0.02	AT
	2.4°/1.7°		0.11	AT	(421)/(11,8,2)	2.7°/6.0°		0.40	AT
	1.3°/1.3°		0.06	AT	(421)/(11,8,2)	2.4°/2.3°		0.02	AT
(332)/(14,11,11)	3.6°/2.9°		0.09	AT	(421)/(11,8,2)	3.5°/2.6°		0.11	AT
(332)/(13,5,2)	4.0°/3.2°		0.28	AT	(421)/(10,8,5)	3.3°/4.1°		0.10	AT
(332)/(13,5,2)	1.6°/3.8°		0.26	AT					
(*b*) CSLs with $5 < \Sigma < 33$									
(110)/(114)	6.7°/2.5°	9	0.48	AT	(110)/(941)	2.7°/6.2°	7	0.63	AT
(111)/(115)	5.1°/6.0°	9	0.22	AT	(711)/(221)	2.0°/3.0°	7	0.50	*P*
(111)/(115)	3.4°/3.0°	9	0.17	AT	*R*/*R*	–	7	0.59	–
(551)/(17,13,1)	0.4°/3.6°	9	0.25	AT	(310)/(27,20,9)	5.0°/2.0°	11	0.67	AT
(111)/(13,7,5)	4.0°/3.3°	9	0.38	AT	*R*/*R*	–	11	0.74	–
(110)/(11,5,4)	1.3°/4.9°	9	0.86	AT	(310)/(851)	3.5°/4.7°	15	0.49	AT
(410)/(410)	3.3°/5.6°	9	0.96	*T*	(210)/*R*	4.9°	15	0.49	–
R/*R*	–	9	0.14	–	*R*/*R*	–	15	0.35	–
(111)/(211)	2.0°/5.6°	27*a*	0.68	*P*	*R*/*R*	–	17*b*	0.70	–
(211)/(331)	3.4°/4.1°	27*a*	0.21	*P*	*R*/*R*	–	19*a*	0.57	–
(510)/(510)	1.0°/2.2°	27*a*	0.68	*T*	(210)/(410)	4.4°/4.6°	21*a*	0.41	*P*
(310)/*R*	5.2°	27*b*	0.86	–	*R*/*R*	–	21*a*	0.50	–
(210)/*R*	0.7°	27*b*	0.34	–	*R*/*R*	–	25*b*	0.72	–
(110)/(211)	4.5°/4.7°	5	0.73	*P*	*R*/*R*	–	33*b*	0.60	–
(311)/*R*	5.4°	5	0.87	–					
Non-CSLs									
(110)/(211)	7.0°/3.7°			*P*	(310)/(210)	4.7°/5.6°			*P*
(113)/(113)	3.9°/3.2°			*P*,*S*	(211)/(311)	2.1°/2.8°			*P*
(310)/(100)	2.9°/4.3°			*P*	(110)/(210)	1.4°/0.3°			*P*
(211)/(211)	4.6°/4.9°			*P*,*S*	(311)/(331)	1.3°/2.6°			*P*

acid to reveal grain boundaries. Orientations from contiguous grains were obtained using an EBSD system interfaced to a JEOL 6400 microscope. Grain-boundary inclinations were obtained using a serial sectioning technique. All five degrees of freedom (misorientation and plane normal) could then be accessed from a combination of the orientation and spatial data. These procedures are described in detail elsewhere (Randle, 1993*a*).

Eleven regions of microstructure were selected at random for measurement. It was neceessary to exclude some boundaries from the sample population because of nonplanarity within the measurement volume. In total, 268 grain-to-grain surfaces (*i.e.* 134 boundaries) comprised the sample population.

3. Results

The grain-boundary geometrical data for the entire sample population are summarized in Table 1. The trends are best highlighted by categorizing the data firstly according to misorientation in three broad divisions: $\Sigma = 3$ CSLs [Table 1(*a*)], CSLs with $5 < \Sigma < 33$ [Table 1(*b*)] and non-CSL [Table 1(*c*)] boundaries; and then categorizing according to plane geometry within each of the three divisions. The proportion of boundaries falling in each of the three groups ($\Sigma = 3$, CSLs with $5 < \Sigma < 33$ and non-CSLs) are 46, 21 and 33%, respectively. Classification of CSLs was based on the Brandon (1966) criterion and boundary planes were allowed a 7° tolerance from the exact orientation (Wolf, 1985). The information contained in each column of Table 1 is as follows.

Column 1. The indices of the nearest low-index boundary plane for both interfacing grains. If there is no low-index plane within 7° of the experimentally determined plane orientation, the plane is irrational and is labelled *R*.

Column 2. The angular deviation from the nearest low-index plane for both interfacing grains.

Column 3. Σ value [Table 1(*b*) only].

Column 4. Angular deviation of the experimentally determined misorientation as a proportion of the maximum allowable deviation for the particular Σ value according to Brandon's criterion (V).

Table 2. *Proportions of STB and ATB* $\Sigma = 3$ *boundaries*

Planes	% of $\Sigma = 3$
(111)/(111)	14.8
(211)/(*uvw*)	11.4
(110)/(411)	9.8
(332)/(*uvw*)	9.8
(310)/(*uvw*)	9.8
(310)/(771)	8.2
(421)/(*uvw*)	8.2
(100)/(221)	4.9

Column 5. Classification of the boundary type: ST (symmetric tilt), AT (asymmetric tilt), *T* (twist), *P* (low-index incommensurate boundary planes), *S* (symmetric).

$\Sigma = 3$ *CSLs*. There are several preferred boundary-plane combinations in this group and these are summarized in Table 2. The most populous is the (111) STB, although the other STB configuration in the $\Sigma = 3$ system, (211), is entirely absent. The vast majority of $\Sigma = 3$ CSLs are ATB. Although there are many possible ATB planar combinations in the $\Sigma = 3$ system, only a few are represented in the present data (see Table 2), indicating some preferred selection. There are no TGBs (twist grain boundaries). For most boundaries in this group, the relative deviation (*V*) from the exact CSL is small (< 0.3, which is 2.5° for $\Sigma = 3$). A very small *V* does not necessarily indicate a low-index boundary-plane combination. For example, the last boundary listed in Table 1(*a*) has $V = 0.01$ and yet has incommensurate boundary planes.

CSLs with $5 < \Sigma < 33$. 28% of boundaries in this group are $\Sigma = 9$'s and all except one are ATBs. The remainder of the group is mixed with respect to distribution of planes: low-index but incommensurate planes, ATBs, TGBs and irrational planes are all represented. Most of the boundaries have a high *V*.

Non-CSLs. Of the non-CSL boundaries, 18% have low-index planes in both grains, 43% have a low-index plane in one grain and 39% have totally random geometries. The low-index plane/non-CSL proportion for the entire sample population is 6%. Only those boundaries having low-index planes in both grains are listed in Table 1(*c*).

Fig. 1 shows examples of the grain structure and grain-boundary geometry in three regions. The grain-boundary plane indices and Σ values (where applicable) for each boundary whose plane orientation was measured are indicated in Fig. 1. Frequently, the distribution of dihedral angles deviates markedly from the equilibrium condition of three grains meeting at an angle of 120° each, which indicates either an inhomogeneous distribution of boundary energy or that equilibrium had not yet been reached. There is also some evidence for the nonrandom spatial occurrence of certain boundary planes; for example, there is a high occurrence of (310) planes in Fig. 1(*a*). The clustering of boundary planes is further highlighted in Fig. 2, which shows, in a standard stereographic unit triangle, the boundary-plane indices for each grain surface.

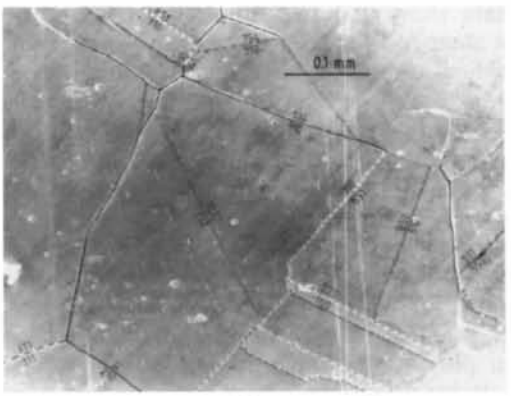

(*a*)

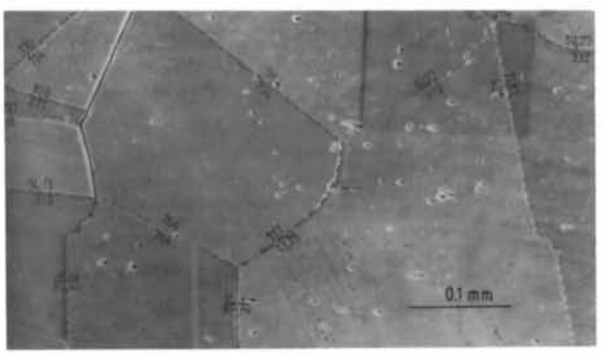

(*b*)

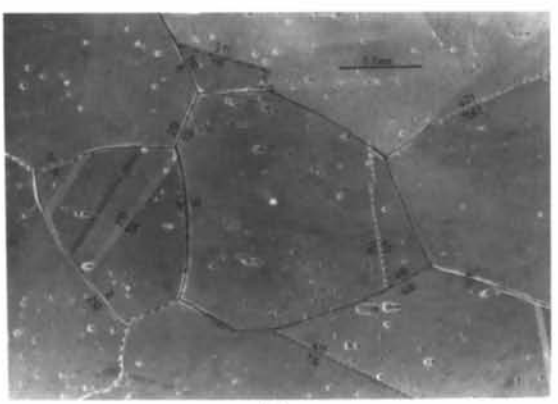

(*c*)

Fig. 1. Grain structures and grain-boundary geometry distributions in three sampled areas. $\Sigma = 3$, $\Sigma = 9$ and non-CSL boundaries are indicated by dotted, dotted-and-dashed and dashed lines, respectively. Boundary planes are labelled by their indices, or by *R* if the boundary plane is irrational, in the crystal systems of both interfacing grains. No boundary-plane measurements were made for unmarked boundaries.

Although there is clearly a trend for variation of planar distributions between the sampled areas, the sample population is not sufficiently large to be statistically significant.

4. Discussion

The data show that two mutually exclusive groups can be identified for grain-boundary plane geometry: tilt configurations for $\Sigma = 3$'s and a small group of low-index grain-boundary planes in both interfacing grains for some non-CSLs. The former group is by far the largest since the sample population is dominated by $\Sigma = 3$'s. The high proportion of $\Sigma = 3^n$ boundaries, particularly where $n = 1$, is common in annealed nickel and has been observed previously (Furley & Randle, 1991; Palumbo & Aust, 1990). Almost all of the $\Sigma = 3$ and most of the $\Sigma = 9$ and $\Sigma = 27$ boundaries are tilt in character, indicating that in polycrystals these are preferred over twists. Previous investigations where grain-boundary plane orientations have been measured in polycrystals concur broadly with the data presented here, although other data sets have been much smaller. In particular, asymmetric $\Sigma = 3$ boundaries occur frequently. An overview of previous data is summarized in Table 3. CSLs other than $\Sigma = 3$ and $\Sigma = 9$ do not show a strong trend towards having 'special' boundary planes. In some cases, although an ATB description can be fitted, one or both planes may be high-index and a more significant description would be to consider proximity to lattice planes. An example is the (111)/(37,23,17) $\Sigma = 27a$ ATB, which can also be described as (111)/(211) [Table 1(*b*)].

Table 3. *Some experimental observations of* $\Sigma = 3$ *plane geometries*

Material	Planes	Reference
Copper	(113)/(335)	Fullman (1951)
Aluminium	(117)/(551), (211)/(211)	Sargent (1968)
Ni–Fe alloy	(533)/(13,13,7), (110)/(110), (153)/(153)	Dash & Brown (1963)
Austenitic steel sheet	(13,5,5)/(11,7,7), (011)/(011)	Vaughan (1970)
Copper sheet (annealed)	Mostly ATBs in (011) zone plus some irrational planes	Omar (1987)
Austenitic steel (recrystallized)	Few $\Sigma = 3$'s; mixed boundary plane types	Randle (1989)
Nickel (specimen 'corner' grains)	Many ATBs in (011) zone plus mixed boundary plane types	Randle & Dingley (1990), Randle (1991)

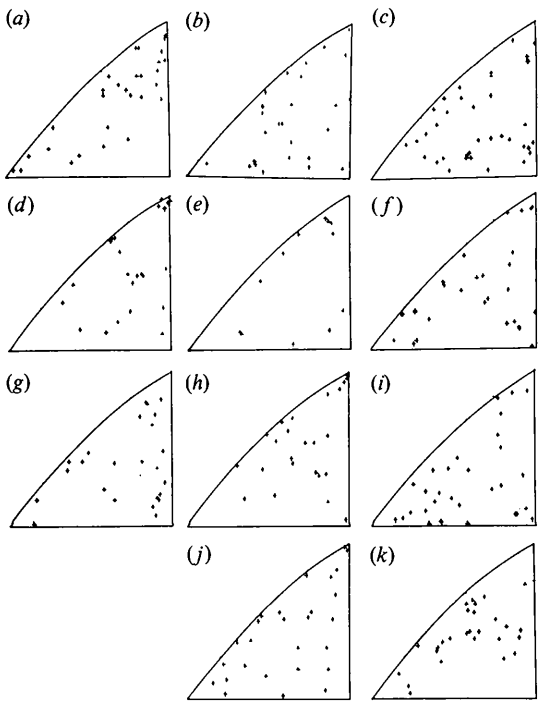

Fig. 2. Distribution of grain-boundary plane indices in a standard stereographic triangle for the entire sample population arranged according to sample area. (*a*), (*b*) and (*c*) correspond to Figs. 1(*a*), (*b*) and (*c*). These distributions show the differences in plane distribution depending on the sampling area.

The overall selection of grain-boundary geometries in the specimen, where substantial grain growth has already taken place, is governed by energy minimization rather than high mobility. In other words, it can be assumed that the trends observed here for boundary geometry selection reflect the lowest-energy condition possible under the constraints imposed by the grain texture, the three-dimensional connectivity in the polycrystal and kinetically controlled processes such as the rate of grain-boundary migration. The total grain-boundary energy in the system can be minimized by reducing the total grain surface area *via* grain growth and removal of grain-boundary curvature in the classical manner and also by maximizing the number of lower-than-average energy boundaries present. The following discussion of the results incorporates the assumption that, within the connectivity constraints of the polycrystal, the data reflect a trend towards energy minimization.

The lowest-energy grain boundary is the $\Sigma = 3$ STB and so it is not surprising that (111)/(111) is the most frequently observed boundary-plane combination. However, as a group, the majority of $\Sigma = 3$'s are ATBs and it is particularly striking that only a few of the possible ATB plane combinations occur in the sample. For example, it might have been expected that the other STB in the $\Sigma = 3$ system, (112)/(112) or the ATB (111)/(115) might have been observed, since low-index lattice planes that give a high *average* interplanar spacing for the two interfacing planes is one criterion for a low-energy boundary (Wolf, 1985). Recent work has shown that in copper the energy of the (112) STB in $\Sigma = 3$ is relatively high and, moreover, the structure of $\Sigma = 3$ boundaries with planes in the (011) zone [*i.e.* the

angle/axis of misorientation is 70.5°/(011)] is a mixture of the structural units associated with the (111) and (112) STBs (Wolf, 1985). This results in a monotonic increase in grain-boundary energy with deviation away from the (111) STB along the (011) zone to the (112) STB (apart from around 82° from the STB, where there is a second energy minimum associated with an atomic rearrangement), as indicated in Fig. 3.

The present data accord well with the low-energy criterion based on deviation away from the (111) STB as in Fig. 3. The deviation from (111) for observed ATBs in the (011) zone (which is proportional to boundary energy) and frequency of occurrence are shown in Fig. 4. The present data are also in agreement with computer simulation and high-resolution microscopy in copper.

There are other $\Sigma = 3$ ATBs in the data set that are not in the (011) zone. For example, (121)/(721) is in the (012) zone: the angle/axis of misorientation is 131.8°/[012]. This ATB has been previously observed in polycrystalline nickel (Randle & Dingley, 1990). Boundaries interfaced by (310) or (421) in one grain are also quite strongly represented in the data set. The occurrence of these boundaries cannot be explained in terms of energy selection since they are predicted to have higher energies than boundary planes in the (011) zone (Wolf *et al.*, 1992). Presumably, all ATBs that deviate from this lower-energy zone could, given sufficient time, alter their inclinations and/or undergo grain rotations towards lower-energy configurations.

Fig. 5 shows the distribution of sampled grain-boundary inclinations expressed as an angular deviation from the upright boundary position, *i.e.* where the boundary is perpendicular to the specimen surface. Grain boundaries at a specimen surface may be expected to behave during annealing differently from those within the bulk. Surface grains have a quasi-two-dimensional nature and boundaries that adjoin the free surface can alter their inclinations readily by virtue of the vacancy supply. This is in contrast to grains within the interior, where grain-to-grain coherency constraints are active in three dimensions rather than two and an external vacancy supply is not available.

Grain boundaries that are perpendicular to and adjoin the specimen surface are in the lowest-energy position because of grain-boundary surface-area minimization criteria. Fig. 5 shows that almost half of the sampled boundaries are nearly parallel (within 10°) to the specimen-surface normal. However, some boundaries deviate quite markedly from this position and there is a direct correlation between the proportion of $\Sigma = 3$ boundaries and the deviation from the lowest-area grain-boundary position. These results are underpinned by previously obtained data on the distribution of grain-boundary planes in nickel where CSL (mostly $\Sigma = 3$'s) and non-CSL boundaries formed two distinct sets with respect to boundary inclination, namely those non-perpendicular and perpendicular, respectively, to the specimen surface (Randle & Dingley, 1989; Randle, 1991). Those data showed a more distinct division between the two inclination groups because the sampled boundaries

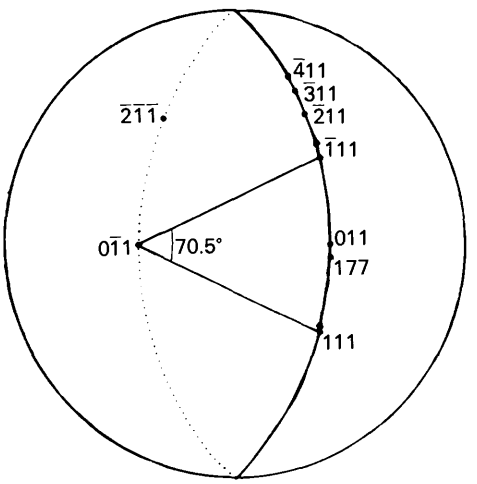

Fig. 3. Stereographic projection illustrating a misorientation of 70.5°/[011] ($\Sigma = 3$) and one symmetric tilt configuration, (111)/(111) planes. Rotations in the (011) zone, in the direction indicated, away from the (111)/(111) ST configuration give rise to many asymmetric tilt configurations. Two examples are shown: (177)/(311) and (011)/(411), which are rotated 29.5 and 35.3° from (111)/(111), respectively. The other STB in the $\Sigma = 3$ system, (211)/(211) [90° from (111)/(111)], is also shown.

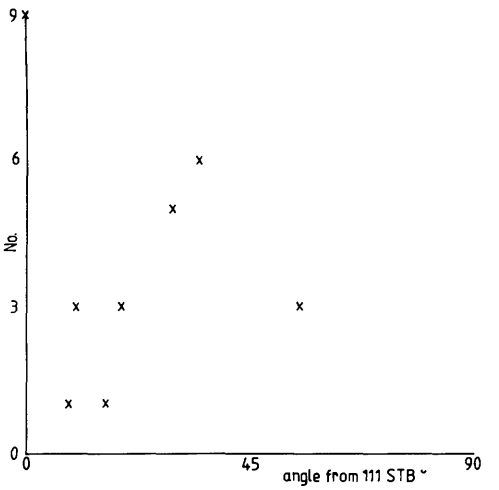

Fig. 4. Boundary planes from the experimental data set that are in the (011) zone, plotted as an angular rotation from the (111) STB. Those boundaries represented, in order of ascending angular rotation, are: (111)/(111), (755)/(23,17,17), (332)/(10,7,7), (221)/(744), (552)/(211), (771)/(311), (110)/(411) and (221)/(100).

all traversed a specimen edge and so had a large amount of rotational freedom. On the other hand, for the present data, the boundary geometry is partially constrained by three-dimensional polycrystal geometry.

The implication from the distribution of boundary inclinations is that a large deviation from the lowest-area (perpendicular to the surface) position is only energetically feasible if the resulting boundary geometry is lower than average. This is supported by the fact that the majority of large inclination boundaries are $\Sigma = 3$. For example, the three boundaries with inclinations $> 50°$ are all $\Sigma = 3$'s. Although Fig. 5 shows that there is some selection of boundary planes *via* inclination and position control, the selection freedom is limited by grain shape and cohesion considerations. Grain orientation is less important in boundary-phase selection, although of course it is the major factor controlling grain misorientation.

Fig. 6(*a*) illustrates schematically an example of inclinations for three boundaries that join at a grain edge (triple junction) as they would be viewed before and after the serial sectioning. It is clear that the constraints are such that it is not possible for only one grain boundary at the junction to be inclined. Furthermore, the direction of the triple junction is fixed by only two of the component boundaries. The third boundary therefore has only one degree of freedom near the junction rather than two since its inclination is fixed as shown in Fig. 6(*b*). However, further away from the junction the boundary may change its boundary plane, either discretely by faceting or continuously by curvature. These are some of the factors that illustrate the space-filling constraints on grains in polycrystals and illustrate why every boundary in a three-dimensional polycrystal does not adopt a low-energy configuration.

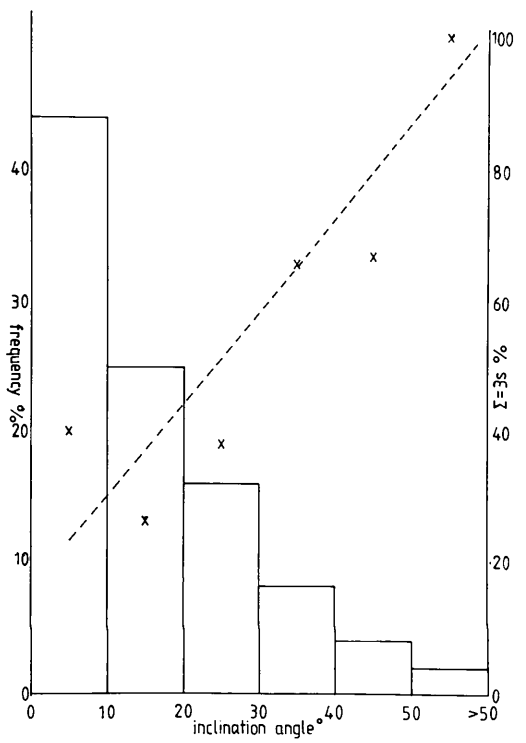

Fig. 5. Frequency distribution of inclination angles of the experimental data set, *i.e.* the angle that each boundary plane makes with the specimen-surface normal. Also included is the proportion of $\Sigma = 3$ boundaries in each inclination angle group. This proportion increases with inclination angle, whereas the overall trend for the total data set is for the inclination-angle frequency to decline sharply with angle magnitude.

5. Concluding remarks

(1) All five degrees of freedom have been measured for a sample population of grain boundaries in polycrystalline annealed nickel using SEM-based techniques.

(2) The data could be divided into three categories: $\Sigma = 3$ CSLs (46%), non-CSLs (33%) and a smaller group of CSLs with $5 < \Sigma < 33$ (21%). Within these categories, the boundaries could be classified according to their boundary planes. Almost all the $\Sigma = 3$ category were either (111) STBs or selected ATBs; 18% of the non-CSLs (6% of the total sampled boundaries) had low-index planes in both grains; the $5 < \Sigma < 33$ group were mixed with respect to boundary planes, except for $\Sigma = 9$'s, which were almost all ATBs.

(3) The inclination of boundaries with respect to the specimen surface was found to correlate with $\Sigma = 3$ CSLs: the greater the angular deviation of the boundary plane away from the specimen surface normal, the higher the proportion of $\Sigma = 3$'s.

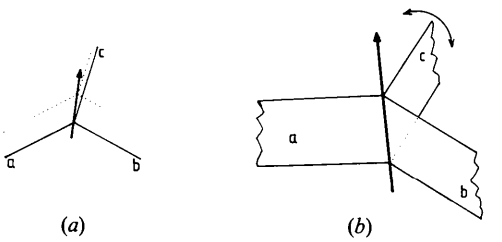

Fig. 6. (*a*) Schematic illustration showing the position of grain-boundary traces before (dotted line) and after (full line) serial sectioning for three boundaries, *a*, *b*, *c*, which meet at a common grain edge (triple junction) shown as a bold arrow (direction arbitrary). It is clear from the diagram that if boundary *a* has a large inclination (shown as a large displacement of the boundary trace before and after sectioning), then at least one of the other boundaries that join in a common direction must also have a large inclination angle. (*b*) Three-dimensional diagram of three grain boundaries with a common edge as in (*a*). The orientation of three boundaries thus joined in a polycrystal is restricted near to the joining line in rotation in the dimension shown.

(4) ATBs were preferred in the polycrystal rather than STBs [except for the (111) $\Sigma = 3$ STB] or TGBs. In particular, ATBs in the $\Sigma = 3$ system in the (011) zone and closer to the (111) STB than the (112) STB occurred frequently. These occurrences could be explained in terms of grain-boundary energy considerations.

References

BRANDON, D. G. (1966). *Acta Metall.* **14**, 1479–1490.
CRAWFORD, D. C. & WAS, G. (1991). *J. Electron Microsc. Tech.* **19**, 345–352.
DASH, S. & BROWN, N. (1963). *Acta Metall.* **11**, 1067.
FULLMAN, R. L. (1951). *J. Appl. Phys.* **22**, 456–460.
FURLEY, J. & RANDLE, V. (1991). *Mater. Sci. Technol.* **7**, 12–19.
OMAR, R. (1987). PhD thesis, Univ. of Warwick, England.
PAIDAR, V. (1987). *Acta Metall.* **35**, 2035–2048.
PALUMBO, G. & AUST, K. T. (1990). *Acta Metall.* **38**, 2343–2352.
RANDLE, V. (1989). *Scr. Metall.* **23**, 773–778.
RANDLE, V. (1991). *Mater Sci. Technol.* **7**, 985–990.
RANDLE, V. (1992). *Microtexture Determination and its Applications*. London: Institute of Materials.
RANDLE, V. (1993*a*). *Grain Boundary Geometry in Cubic Polycrystals*. Bristol: Institute of Physics.
RANDLE, V. (1993*b*). Proceedings of Conference on Grain Boundary Engineering, Kingston, Canada. In the press.
RANDLE, V. & DINGLEY, D. J. (1989). *Scr. Metall.* **23**, 1565–1570.
RANDLE, V. & DINGLEY, D. J. (1990). *Proceedings of EUROMAT 89, Advanced Materials and Processes*, edited by H. E. EXNER & V. SCHUMACHER. Oberusel: DGM.
SARGENT, C. M. (1968). *Trans. Metall. Soc. AIME*, **242**, 1188–1191.
VAUGHAN, D. (1970). *Philos. Mag.* **40**, 1003–1011.
WOLF, D. (1985). *J. Phys.* **46**, *Colloq.* C4, 197–208.
WOLF, U., ERNST, F., MUSCHIK, T., FINNIS, M. W. & FISCHMEISTER, H. F. (1992). *Philos. Mag.* A**66**, 991–1016.

Acta Cryst. (1994). A**50**, 595–601

Probabilistic Estimation of the Structure Seminvariants in the Monoclinic and Orthorhombic Systems when Anomalous Scatterers are Present

BY YONG-SHENG LIU AND NING-HAI HU

Applied Spectroscopy Laboratory, Changchun Institute of Applied Chemistry, Chinese Academy of Sciences, Changchun 130022, *People's Republic of China*

(*Received* 29 *October* 1993; *accepted* 15 *March* 1994)

Abstract

The estimate formulas for the two-phase structure seminvariants (TPSSs) in the presence of anomalous scattering are obtained from the estimate of the two-phase structure invariants [Hauptman (1982). *Acta Cryst.* A**38**, 632–641; Giacovazzo (1983). *Acta Cryst.* A**39**, 585–592] and the conditional probability distribution of the TPSSs is derived from the neighborhood theory [Hauptman (1975). *Acta Cryst.* A**31**, 680–687]. A procedure for estimating the one-phase structure seminvariants near 0 or π (OPSSs) is proposed, based on the TPSS estimates. Test results for known structures with error-free data show accurate estimates for the TPSSs, even in the macromolecular case. For the OPSSs, the accuracy is related to the strength of anomalous scattering by heavy atoms in the macromolecular case. The incorporation of the heavy-atom information improves the results.

1. Introduction

In about the past ten years, the combination of traditional direct methods with anomalous dispersion has been extensively studied to improve the methods for phase determination of macromolecular structures. Hauptman (1982*b*) proposed the probabilistic theory of the two- and three-phase structure invariants by integrating anomalous-dispersion effects into the neighborhood concept. Giacovazzo (1983) also obtained a similar result by a different route. Fortier, Fraser & Moore (1986) later re-examined the theoretical basis for this approach and obtained more-accurate three-phase-invariant estimates by the use of anomalous-scatterer substructure information. Subsequently, Hao & Fan (1988) presented a method for the individual phase estimates by the incorporation of heavy-atom information into Hauptman's distribution.

The estimate of the two-phase structure invariants (TPSIs) arose from the joint probability distribution of the Friedel pair $E_{\mathbf{H}}$ and $E_{\overline{\mathbf{H}}}$ in the presence of anomalous scattering. The practical application of this result has been suggested by Cascarano & Giacovazzo (1984). Further studies of the TPSIs can be found in other publications (Guo & Hauptman, 1989; Guo, 1990; Guo, Blessing & Hauptman, 1991).

In research into structure seminvariants, Velmurugan & Hauptman (1989) derived the conditional probability distribution for the OPSSs having